



# Blue-green light emitting inherent luminescent glasses synthesized from agro-food wastes

Shivani Punj<sup>1</sup> · K. Singh<sup>1</sup>

Received: 25 October 2018 / Accepted: 2 January 2019 / Published online: 7 January 2019  
© Springer Science+Business Media, LLC, part of Springer Nature 2019

## Abstract

Silica-phosphate glasses are synthesized using various agro-food wastes as resource materials instead of minerals. These glasses are synthesized using the melt-quench technique. These as prepared glasses are characterized by X-ray diffraction analysis, Energy dispersive spectroscopy, Fourier transform infrared spectroscopy, UV–Visible and photoluminescence techniques. The X-ray diffraction showed the amorphous nature of the prepared samples. The presence of elemental composition and inherent trace elements such as  $\text{TiO}_2$ ,  $\text{Fe}_2\text{O}_3$  determined using energy dispersive spectroscopy. The density and vicker micro hardness of these glasses have been increased by increasing of egg shell powder contents (CaO). The hardness of the present samples is higher than earlier reported similar type of glasses. The presences of Si–O–Ca and Al–O–Ca groups in the glass are identified. The presences of different silicate-phosphate units are also observed. The optical band gap of these glasses lies in the range 3.63–3.84 eV. The refractive index and photoluminescence of these glasses have been also increased by increasing of CaO content in the glasses.  $\text{TiO}_4$  is a “self activating” anion which helps to improve the luminescent quality of these glasses. The color purity is 66% of these glasses. The presences of inherent trace element oxides are responsible for good photoluminescence properties of the present glasses.

## 1 Introduction

Agricultural and food wastes are increasing with increasing the population of the world. One-third of agricultural wastes ashes are usually dumped in various places which create lots of environmental problems [1]. It is an important and necessary to utilize the wastes ashes in a meaningful way to protect the environment as well as human health. Present times, few amounts of agricultural and food wastes are being used as constructions, biodiesel, fuel, fertilizers and electricity generation [2–5]. Agro-food wastes could also be used as resource materials to make silicate based glasses/glass–ceramics because these wastes have  $\text{SiO}_2$ , CaO,  $\text{Na}_2\text{O}$  etc. that are usually required to make silicate glasses and glass ceramics [6]. The addition of alkali metal oxides and trivalent oxides particularly rare earth oxides affect the local glass structure as well as luminescence properties of the glasses. Because each alkali and alkaline earth metal

ions have in different field strengths, ionic radii ratios and coordination numbers in the glass structure.

Some researchers have reported the agro-food wastes such as rice husk, wheat straw, sugarcane baggase, can be used to extract silica [7, 8]. Corn husk ashes (CHA) contain  $\text{SiO}_2$  (35 wt%),  $\text{P}_2\text{O}_5$  (22.5 wt%),  $\text{K}_2\text{O}$  (20.2 wt%) along with some oxides of trace element [6]. On the other hand, sugarcane husk ashes (SCLA) and eggshell powder (ESP) are also good sources of  $\text{SiO}_2$  and CaO respectively. Phosphate glasses become an important area for different applications such as optical amplifiers, fibers, laser and biomedical applications etc. [9–11]. But its poor chemical durability makes them ineffective [12]. The chemical durability can be improved by adding some alkaline earth metal oxides and adding  $\text{Al}_2\text{O}_3$  because  $\text{Al}^{3+}$  ions acts as cross linkers between chains [13]. SCLA contain the maximum amount of silica (70–75 wt%) along with some trace elements such as  $\text{Al}_2\text{O}_3$ ,  $\text{TiO}_2$  and  $\text{Fe}_2\text{O}_3$  [13]. ESP has a rich amount of alkaline earth metal oxides such as CaO (98 wt%) and with some trace element oxides. ESP helps to reduce the melting point and improve chemical durability of silica-phosphate glasses, especially for biomedical applications [14].

In recent times, our group has reported that agro wastes such as rice husk, wheat straw and sugarcane baggase can

✉ K. Singh  
kusingh@thapar.edu

<sup>1</sup> School of Physics and Materials Science, Thapar Institute of Engineering and Technology, Patiala 147004, India

be used as resource materials, instead of conventional oxides to synthesize glasses and glass ceramics. Danewalia et al. [15] studied structural and dielectric properties of glass/glass–ceramics derived from rice husk and sugar cane leave ash synthesized by melt quench method. The results indicated that the addition of sugarcane leaves ash increase the tendency of glass formation. These as prepared glasses were inherently porous, which was responsible for low dielectric permittivity i.e. 9–40 at room temperature and 100 Hz. Sharma et al. [16] have studied optical and thermal properties of glasses/glass–ceramics using agriculture wastes. The results indicated that optical band gap of as-quenched samples were in wide-band gap semiconductor range, i.e. 3.49–4.17 eV. The coefficient of thermal expansion (CTE) is in the range of  $13\text{--}16 \times 10^6 / ^\circ\text{C}$ .

Devi et al. [17, 18] reported the structural and luminescence properties of  $\text{Ca}_2\text{SiO}_4$  doped with  $\text{Dy}^{3+}$  and  $\text{Eu}^{3+}$  phosphors using rice husk ash and egg shell powder as resource materials. The results showed single phase monoclinic structure for both the phosphors. Phosphors  $\text{Dy}^{3+}$  showed blue–yellow emission spectra. This was due to energy transfer between  $\text{Dy}^{3+}$  ions by dipole–dipole interactions.  $\text{Eu}^{3+}$  phosphor showed emission in the deep red region due to high intense emission of  $^5\text{D}_0 \rightarrow ^7\text{F}_4$  at 703 nm. Aktas et al. [19, 20] studied structural, optical and mechanical properties using peanut shell powder (PSP) doped in soda lime silica (SLS) glasses prepared by the melt–quench technique. The UV–Vis spectroscopy results indicated that the light transmitted by the SLS glass decreased and became dark green with increasing PSP content ( $\geq 1$  wt%), due to the presence of  $\text{Fe}_2\text{O}_3$  in PSP contents. The micro hardness and fracture toughness also increased of SLS glass samples due to the presence of CaO (29.7 wt%) in the PSP. Teixeira et al. [21] developed glass–ceramics using sugarcane baggase ash and reported their structural and mechanical properties. The results indicated wollastonite ( $\text{CaSiO}_3$ ) as the major crystalline phase and higher value of micro hardness i.e. 564 HV. Some of the agro–food wastes exhibit some trace element oxides. These trace element oxides may act as luminescent species if it is used as resource materials. Thus, agro–food wastes can be used to synthesize value added glasses and glass ceramics for engineering applications. These glasses could be replaced the conventional glasses that synthesized from conventional oxides. In addition to this, these glasses have some advantages over conventional glasses since they have some amount of transition and heavy metal oxides as trace element oxides inherently. So, the presence of these inherent trace element oxides acts as active centers for photoluminescence in agro–food waste derived glasses and glass ceramics.

The main objective of the present study is to develop luminescent glasses by keeping fixed composition of CHA and SCLA replaced by ESP. Moreover, as per our knowledge

**Table 1** Elemental chemical composition of all the raw materials using for glass preparation

Elements	CHA (wt%)	SCLA (wt%)	ESP (wt%)
Si K	3.72	36.24	0.07
Na K	6.64	0.30	–
Ca K	3.97	2.99	70.21
P K	2.06	–	0.02
Mg K	6.61	3.87	0.63
K K	37.09	8.19	–
Al K	2.94	–	0.03
Ti K	–	0.41	–
Fe K	4.26	0.62	–
O K	32.71	47.38	29.04

The data is obtained from EDS

**Table 2** Density of as prepared glass samples

Sample ID	CHA (wt%)	SCLA (wt%)	ESP (wt%)	Density (g/cc)
CSE-1	60 gm	30 gm	10 gm	2.46
CSE-2	60 gm	20 gm	20 gm	2.57
CSE-3	60 gm	10 gm	30 gm	2.70

corn husk ashes have not been reported to make glasses/glass–ceramics. The prepared glasses are characterized by various techniques to study their structural and photoluminescence properties.

## 2 Materials and methods

### 2.1 Glass sample preparation

The presence of different elements and their amounts in raw materials (CHA, SCLA and ESP) were given in Table 1. Three glass samples were prepared using different weight percent of CHA, SCLA and ESP. Glass composition was selected as [60CHA-(40-x)SCLA-(x)ESP] where,  $x = 10, 20, 30$ . The glass samples were designated as CSE-1, CSE-2 and CSE-3 also shown in Table 2. The ashes of different samples were calcined at different temperatures such as CHA was calcined at 500 °C for 5 h (h) and SCLA at 1000 °C for 2 h. Egg shells were taken, washed with distilled water to remove impurities from it and kept in a 1 M HCl solution for 2 h. Then, the eggshells were washed again with distilled water. Then, egg shells kept in oven at 70 °C for 6 h to make it totally dry. Finally, egg shells ground in an agate mortar to convert in powder. The calcined powder of different ashes and egg shell powder mixed in an agate mortar pestle for 2 h. After grinding, the mixture was put into recrystallized

alumina crucible and melted at 1550 °C at a heating rate 5 °C min<sup>-1</sup> in a programmable furnace. At 1550 °C, the samples were kept for 0.5 h to get homogeneous melt. The melt was quenched in air using thick copper plates. The as quenched samples were crushed into powder for further investigation.

## 2.2 Characterizations

The density of the quenched samples was determined by Archimedes' principle at room temperature with xylene as reference using a sensitive microbalance (Mettler Toledo). The least count of the balance was 0.01 mg. The densities of the samples were calculated as follows:

$$\rho_{sample} = \frac{w_a}{w_a - w_x} \times \rho_x$$

Where  $\rho_{sample}$  density of the sample,  $\rho_x$  is the density of xylene at room temperature,  $w_a$  is the weight of the sample in air and  $w_x$  is the weight of xylene. Density of xylene is 0.863 g/cc at room temperature. The X-ray diffraction (XRD) analysis of all powder samples was obtained from Philips X'Pert e PRO PANalytical using Cu-K $\alpha$  source ( $\lambda = 1.54 \text{ \AA}$ ) between the diffraction angles 10° to 90° that operating at 30 kV and 15 mA. During the experiment, the step size was 0.02° and scan rate was ~1.25°/min. FTIR was carried out at room temperature in the region 4000–400 cm<sup>-1</sup> using Perkin Elmer Spectrum RX (1) spectrometer. Approximately 0.5 mg of each sample was mixed with 20 mg of KBr in an agate mortar and then this powder was used for recording the transmission spectra. Energy dispersive spectroscopy (EDS) analysis was carried out on the raw materials as well as quenched glasses to know the presence of different element oxides (Oxford Instruments INCA-Act Energy 200). Vickers micro hardness of glass samples was calculated using the model (Mitutoyo MVK-HO, Japan) from the indentations using the formula;  $H = 1.854 L/d^2$ , Where HV is the Vickers hardness number, L is the applied load in kg and d is the diagonal length of the square indentation in mm. A 500 gm load is applied to the samples for 15 s. The optical band gap of glass samples was recorded using double beam UV–Visible spectrophotometer in diffused reflectance mode (model: HITACHI U-3900 H) within the wavelength range of 200–800 nm. Scanning speed was 120 nm/min and resolution of the instrument was 0.20 nm. PL spectroscopy was used to study the luminescence properties of the glass samples. PL excitation and emission spectra of all samples were recorded at room temperature in the fluorescence mode with a fluorescence spectrophotometer using Model-Agilent Carry Eclipse G9800A with a xenon flash lamp.

## 3 Results and discussions

### 3.1 Density

The apparent density of the prepared glasses lies in the range from 2.46 to 2.70 g/cc. The density of the glasses (Table 2) increased on replacing SCLA by ESP. As network modifier increases, the modifier ions occupy the interstitial sites within the glass network leads to increase the density. The density of glass samples is comparable to earlier reported conventional glasses, such as 45SiO<sub>2</sub>–25CaO–10Na<sub>2</sub>O–5P<sub>2</sub>O<sub>5</sub>–15TO, doped with TiO<sub>2</sub>, MnO<sub>2</sub>, Fe<sub>2</sub>O<sub>3</sub> and ZnO [22]. The density of conventional glasses has higher values, i.e. 2.75 g/cc, 2.83 g/cc, 3.02 g/cc and 2.98 g/cc respectively. The reason of lower density of present glass samples may be due to the presence of inherent porosity lead to increase the overall volume of the glasses.

### 3.2 XRD analysis

The amorphous nature of as prepared samples was confirmed by X-ray diffraction. XRD patterns of three powder samples do not reveal any sharp peaks which is an indication of absence of crystalline phases in all the samples. All the samples exhibit a broad hump centered on ~29° as shown in Fig. 1. The position of broad humps depends on the initial constituents of the samples.

### 3.3 EDS analysis

The EDS analysis was done on the raw materials as well as quenched glasses. A representative EDS spectrum of CSE-1 glass is given in Fig. 2. SiO<sub>2</sub>, CaO, P<sub>2</sub>O<sub>5</sub>, K<sub>2</sub>O, MgO and some trace element oxides are also present as shown in Table 3. As egg shell powder added to the cost of SCLA,

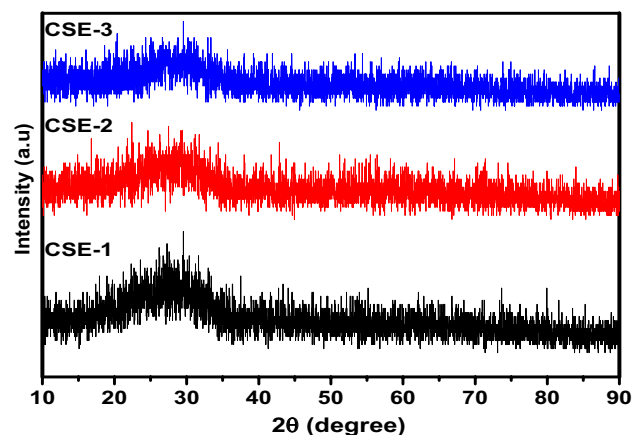


Fig. 1 XRD patterns of as quenched samples

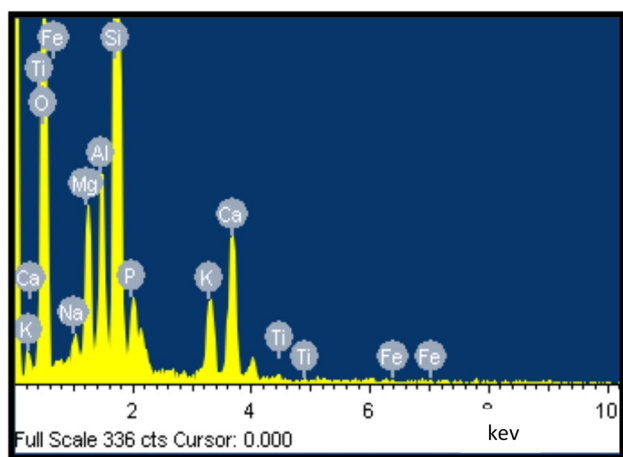


Fig. 2 Representative EDS spectrum of CSE-1 glass sample

both the primary glass former ( $\text{SiO}_2$ ,  $\text{P}_2\text{O}_5$ ) decreases in CSE-2 and CSE-3 glasses. On the other hand modifiers CaO,  $\text{K}_2\text{O}$  and intermediate oxide  $\text{Fe}_2\text{O}_3$  increases, whereas, other modifiers such as  $\text{Na}_2\text{O}$  and  $\text{MgO}$  decreases. The content of  $\text{TiO}_2$  and  $\text{Al}_2\text{O}_3$  did not show any trend in the present glasses. Good amount of  $\text{Al}_2\text{O}_3$  is also present as shown in Table 3. This is picked up from the crucible as glasses are melted in recrystallized alumina intentionally. Basically,  $\text{Al}_2\text{O}_3$  increase the durability of the glasses and prevent non-radiative decay which leads to increase PL intensity in silica–phosphate glasses.

### 3.4 FTIR analysis

FTIR spectra of the samples manifest the stretching and bending bonds of the constituents. The FTIR spectra show the bands at 3624, 1802, 1035, 764, 560 and 470  $\text{cm}^{-1}$ . The band around 3624  $\text{cm}^{-1}$  corresponds to the H–O–H attributed the stretching vibrations of absorbed water molecules. It is assumed that the glasses absorbed atmospheric moisture during the sample preparation for FTIR measurement. This band becomes prominent as an ESP content increase in the glasses. It indicates that ESP addition increase the tendency of water absorption of the present glasses. It is particularly good sign that the present glasses could be used as bioceramics since their glass surface enhance the tendency to form the silanol group responsible for the hydroxyapatite layer formation [23]. Another broad band centered at 1802  $\text{cm}^{-1}$

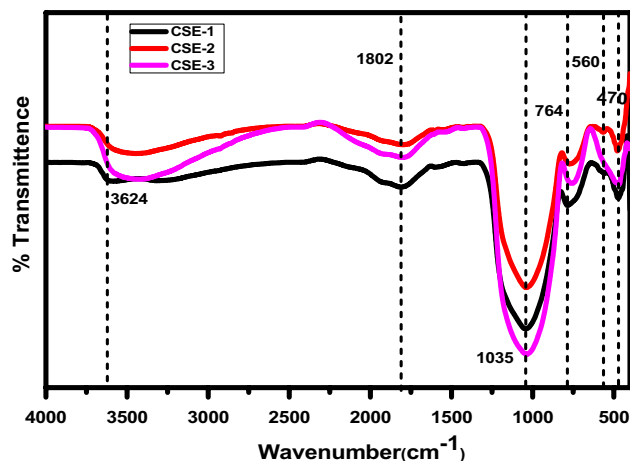


Fig. 3 FTIR transmission spectra of all glass samples

corresponding to stretching mode of Si–OH group [24]. The most intense and broad IR bands occurs at 1035  $\text{cm}^{-1}$  corresponding to the vibrations of  $[\text{SiO}_4]^{4-}$  and  $[\text{PO}_4]^{3-}$  which may overlap one another. Similar results have also been reported by Singh et al. [25] for mineral glasses. The reason of broadness of this band is due to the presence of different silicate units. The band at 764  $\text{cm}^{-1}$  show combined effect for Si–O–Si bending vibration and Si–O–Al stretching mode. This band is more prominent in CSE-3 glass. It is confirmed that these glasses exhibit the contents of  $\text{Al}_2\text{O}_3$ . It is also reported by EDS analysis (Table 3). It can be seen that with increasing ESP contents on replacing SCLA, the concentration of  $\text{SiO}_2$  decreases in the glasses and position of these band shifts towards lower wavenumber. Bands at 470  $\text{cm}^{-1}$  corresponds to bending vibrations of  $\text{SiO}_4$  tetrahedra. It indicates that silica is formed the glass network [26]. Another band at 560  $\text{cm}^{-1}$  is related to asymmetric bending vibrations of P–O bonds. The FTIR spectra and EDS results are consistent to confirm that  $\text{P}_2\text{O}_5$  also present in the glasses. By increasing the contents of ESP in the glass structures the intensity of P–O–P bending band is decreased. The content of  $\text{P}_2\text{O}_5$  is also decreased as observed in EDS analysis (Table 3). This is due to the presence of the network modifiers results in disrupting the continuity of the glass network, this increases the number of NBO groups, which changes the glass structure. So, lead to change the nature of P–O–P band as observed in Fig. 3. The deconvolution was done on broad spectra of the glasses to distinguish the silicate units. The deconvolution spectra of the glasses is

**Table 3** The chemical composition (wt%) of all glass samples. Elemental wt% convertor in oxides using INCA software which is inbuilt in EDS set up

Samples ID	$\text{SiO}_2$	$\text{Na}_2\text{O}$	CaO	$\text{P}_2\text{O}_5$	MgO	$\text{K}_2\text{O}$	$\text{Al}_2\text{O}_3$	$\text{TiO}_2$	$\text{Fe}_2\text{O}_3$
CSE-1	55.02	1.48	13.90	5.27	7.25	6.36	9.97	0.20	0.63
CSE-2	51.43	0.96	16.50	5.19	7.16	6.55	11.36	0.27	0.65
CSE-3	47.86	0.83	23.49	4.55	6.41	6.96	8.05	0.15	1.42

showing six bands i.e.  $733\text{--}724\text{ cm}^{-1}$ ,  $870\text{--}861\text{ cm}^{-1}$  ( $Q^0$ )  $915\text{--}906$  ( $Q^1$ )  $\text{cm}^{-1}$ ,  $1035\text{--}1012\text{ cm}^{-1}$  ( $Q^2$ ),  $1173\text{--}1153\text{ cm}^{-1}$  ( $Q^3$ ) and  $1208\text{--}1205\text{ cm}^{-1}$  ( $Q^4$ ). These bands are corresponding to the discrete anionic structural units such as 3D networks; sheets, infinite chains, dimmers and monomers with non bridging oxygen's versus silicon ratio of  $Q^0$ ,  $Q^1$ ,  $Q^2$ ,  $Q^3$  and  $Q^4$  respectively. All bands mentioned in the spectra are slightly different to each other as shown in Fig. 4. The bands  $870\text{--}861\text{ cm}^{-1}$  are corresponding to  $\text{Si-O}^-$  stretching vibrations mode in  $Q^0$  units in the silicon oxygen sub networks. The band near  $915\text{--}906\text{ cm}^{-1}$  is corresponding to asymmetric stretching vibrations  $\text{Si-O-Si}$  and  $\text{P-O-P}$  mode. Broad band

at  $1035\text{--}1012\text{ cm}^{-1}$  corresponds to stretching vibrations of  $\text{Si-O}^-$  bond in the  $Q^2$  structure of the silica network [27]. A shoulder at  $1173\text{--}1153\text{ cm}^{-1}$  is related to asymmetric stretching vibrations of  $\text{Si-O-Si}$  and  $\text{P-O}$  groups to  $Q^3$  unit [28]. A band at range  $1208\text{--}1205\text{ cm}^{-1}$  is of  $Q^4$  unit corresponding to stretching vibration mode of  $\text{Si-O-Si}$  and  $\text{O-P-O}$  bridging unit. The deconvolution fitting indicates that the intensities of all bands in CSE-2 sample decrease as compared to other glass samples. This may be due to the presence of higher contents of intermediate oxide i.e.  $\text{Al}_2\text{O}_3$  as compared to  $\text{Na}_2\text{O}$ ,  $\text{MgO}$  and  $\text{K}_2\text{O}$ . With the increase in  $\text{Al}_2\text{O}_3$  content, there may have more  $\text{Al-O-Si}$  or  $\text{Al-O-P}$  linkages in the glasses. The relative

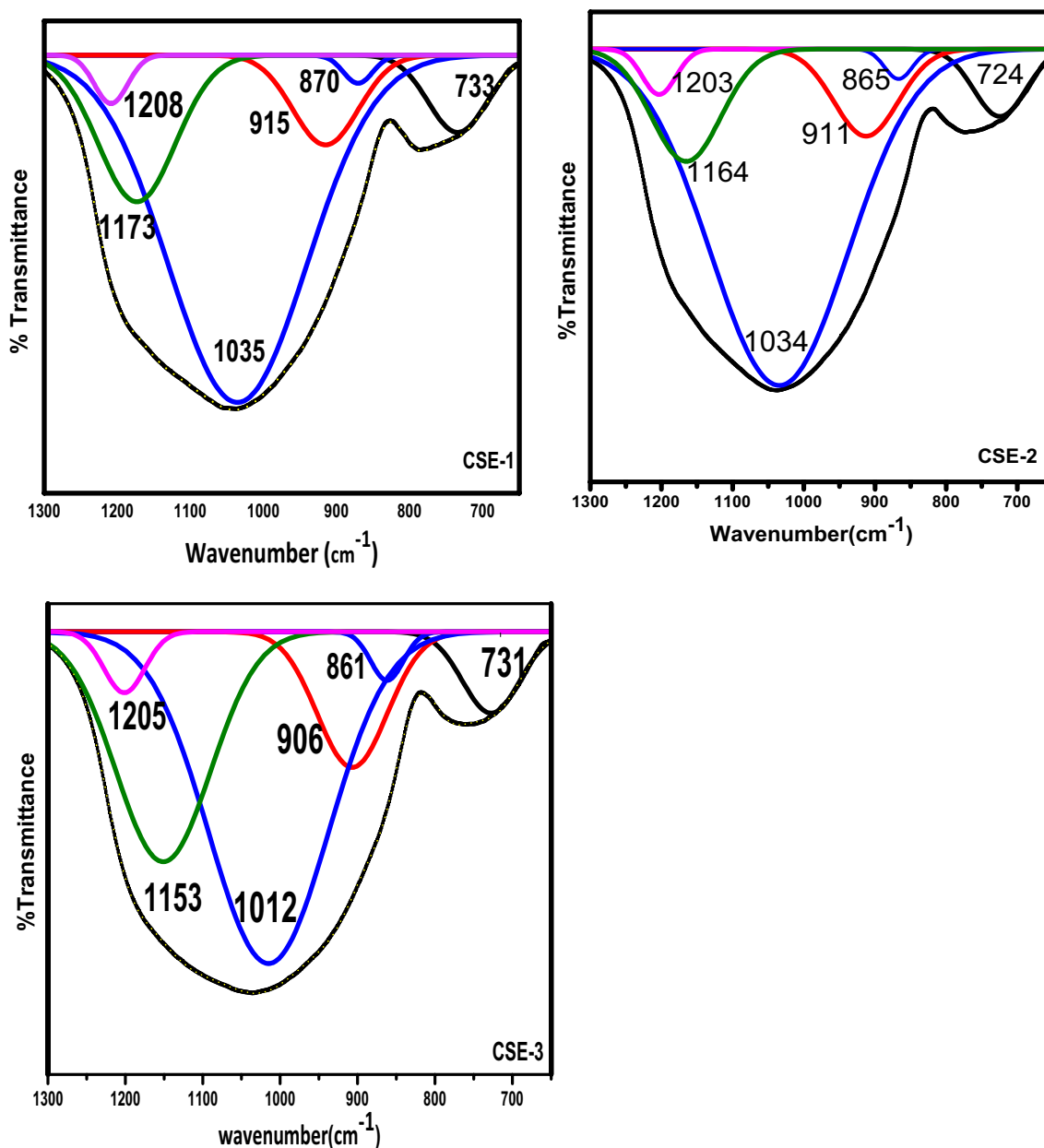


Fig. 4 Deconvolution spectra by peak fitting method using Gaussian curves of all glass samples in the wave number of  $700\text{--}1300\text{ cm}^{-1}$

area of bands are decreasing in the range of 866–912  $\text{cm}^{-1}$  and 1153–1205  $\text{cm}^{-1}$ . On the other hand, the relative area corresponding to band 1035  $\text{cm}^{-1}$  increasing in CSE-2 glass. In case of a CSE-3 glass, band occurs at around 1153  $\text{cm}^{-1}$  due to asymmetric stretching of Si–O–Si and P–O units. It showed maximum intensity as compared to CSE-1 and CSE-2 glasses. This band corresponds to the  $Q^3$  unit that form the inter linkage of one  $\text{SiO}_4$  group with another  $\text{SiO}_4$  tetrahedron. It may also relate to  $\text{SiO}_4$  tetrahedron with an  $\text{AlO}_4^-$  group. All these  $\text{SiO}_4$  and  $\text{AlO}_4^-$  tetrahedral form the glass network in alumina silicate glasses due to the presence of  $\text{Al}^{3+}$  in four fold coordination [29]. The  $\text{AlO}_4^-$  needs charge balancing in spite of  $\text{SiO}_4$  tetrahedral. In this case  $\text{Ca}^{2+}$  may play dual role as modifiers and charge balancing in  $\text{AlO}_4^-$  units. So  $\text{Ca}^{2+}$  plays the role of network modifiers to form more NBOs. Similarly the presence of some other network, modifying oxides can also disrupt the BOs of Si–O–(Si, Al) bond leads the formation of NBOs. The intensity of all bands in CSE-three glass is increased relates due to breaking of Si–O–Si and P–O–P bonds in the glass network. It is taken place due to increase of CaO contents and some other modifiers. The NBOs may be increased due to Si–O–Ca, Al–O–Ca bonds in the glasses. So, the relative area of these bands is increased. The full width at half maxima in the CSE-3 glass is also increased as compared to two other glasses (Table 4). The FWHM increases with increase of cation field strength due to the presence of modifiers. This indicates that degree of disorderness increases due to changes in the distributions of the Si–O $^-$  and P–O bonds. The vibrational frequency of molecular units is directly related to force constant which associated with cation–anion bonds [30]. The bond length of Si–O $^-$  can be calculated by using stretching vibrational modes and force constant, K. The K is correlated to the average bond distance ( $r$ ) by the following relation:-

$$K = \frac{17}{r^3} \quad (1)$$

K is determined by using

$$\nu = \frac{1}{2\pi c} \sqrt{\frac{k}{u}} \quad (2)$$

**Table 4** Deconvolution parameters of glasses in wave number of 700–1300  $\text{cm}^{-1}$

CSE-1			CSE-2			CSE-3		
C	A	FWHM	C	A	FWHM	C	A	FWHM
733	6.1	94.9	724	5.1	85.68	731	5.7	86.9
870	1.1	47.2	866	1.2	45.9	861	1.9	49.4
915	7.9	105.5	912	8.3	106.2	906	11.6	107.3
1035	64.9	222.2	1034	68.7	227.2	1012	48.5	181.9
1173	15.3	123.9	1165	11.6	114.6	1153	26.6	143.9
1208	2.2	53.4	1203	2.3	55.4	1205	3.0	62.0

C is the band center ( $\text{cm}^{-1}$ ) of the component bands, A is the relative area and FWHM is full-width at half maxima

where  $\nu$  is the frequency of vibration,  $c$  is the velocity of light, and  $\mu$  is effective mass of the units.

Two body reduced mass is

$$\frac{M_{\text{Si}}M_{\text{O}}}{M_{\text{Si}} + M_{\text{O}}} \quad (3)$$

where  $M_{\text{Si}}$  and  $M_{\text{O}}$  are the atomic weights of Si and O. The calculated force constant for  $\text{SiO}_2$  units and bond distance values is given in the Table 5. The change in force constant confirmed that bridging oxygen converted into non bridging oxygen with increasing contents of ESP.

The decrease in intensity of deconvoluted bands is probably related to lowering of the network dimensionality. This is caused by the addition of modifiers and intermediate oxides like  $\text{Al}_2\text{O}_3$ . The increase in intensity is related to a breaking of Si–O–Si and P–O–P bonds in the glass network. It is concluded that the changes in their peak positions shifts towards smaller wavenumber due to change among  $Q^0$ ,  $Q^1$ ,  $Q^2$ ,  $Q^3$  and  $Q^4$  units and their amount in the glasses.

### 3.5 Hardness

The hardness is very complex property which depends upon different factors such as bond strength, porosity, degree of polymerization and fictive temperature [31]. Hardness also provides information about the compactness of the materials. When SCLA is replaced by ESP the micro hardness value of the glass samples showed an increasing trend. It lies in the range 575–638 HV as shown in Table 5. The Vickers's

**Table 5** Calculated force constant and bond distance of glasses using the most intense bands along with micro hardness

Sample ID	Wavenumber ( $\text{cm}^{-1}$ )	K (N/m)	R ( $^\circ$ )	Micro hardness (HV)
CSE-1	1035	387.5	3.52	575 $\pm$ 0.04
CSE-2	1034	386.8	3.53	583 $\pm$ 0.07
CSE-3	1012	370.5	3.57	638 $\pm$ 0.01

hardness of the oxide glasses is ~2–8 GPa [32]. Researchers have earlier reported maximum value of micro hardness to be 574 HV using ESP in soda lime silicate glasses. In the present study, maximum obtained value of the hardness is 638 HV. The higher contents of the ESP (CaO) can increase the non bridging oxygen by disrupting the silica and phosphate network chains as also observed in FTIR spectra. This leads to compacting of the local glass structure. It can also be said that with the increasing concentration of the modifiers the packing of the molecules becomes denser. Another reason may be the presence of CaO (3.35 g/cc) has a high density as compared to SiO<sub>2</sub> (2.65 g/cc). The higher ESP (CaO) contents make the glass structure more rigid, resulting in higher hardness. This results in increase of micro hardness with increase of CaO contents due to densification. Conventional phosphate-soda glasses containing Li<sub>2</sub>O or K<sub>2</sub>O as modifiers showed the maximum value of Vickers hardness i.e. 630 HV [33]. It was observed that glasses with higher contents of CaO and lowest contents of Na<sub>2</sub>O have the highest value of hardness in these glasses. Jha et al. [34] reported the hardness in the range of 464–502 HV for 55SiO<sub>2</sub>–10K<sub>2</sub>O–(35-x) CaO–x–MgO mineral based glasses. The value of hardness increases with replacement of CaO by MgO due to the higher field strength of Mg<sup>2+</sup> (0.45A<sup>0</sup>) than Ca<sup>2+</sup> (0.33A<sup>0</sup>). Thus, it is concluded that the increase in the compactness of the glass structure is due to the presence of mixed modifier ions present in these glasses.

### 3.6 UV/Visible spectroscopy

#### 3.6.1 Optical band gap and Urbach energy

Optical band gap can be determined using Kubelka–Munk function, F(R) in diffused reflectance mode for solid samples [35].

$$F(R) = \frac{(1 - R)^n}{2R} \tag{4}$$

where R is reflectance and n is the index whose value depends on the type of transition takes place (where n = 1/2, 2, 3/2 and 3 for direct allowed, indirect allowed, direct forbidden and indirect forbidden transitions respectively). The present glasses are opaque in nature. The glass samples reflectance increases with increase of the ESP contents CSE1 > CSE2 > CSE3 as given inset of Fig. 5. On the other hand, their transparency decreases with ESP content. The optical band gap is calculated using tauc plot as shown in Fig. 5. By plotting the graph between (F(R).E)<sup>2</sup> and energy (E) extra plotting the linear region of curves to E (E = hv) axis for CSE-1, CSE-2 and CSE-3. The lowest optical band gap is observed in the CSE-3 glass sample as shown in Table 6. As SCLA is replaced by the ESP up to 30 wt% the optical band gap of the glasses is decreased. The value of

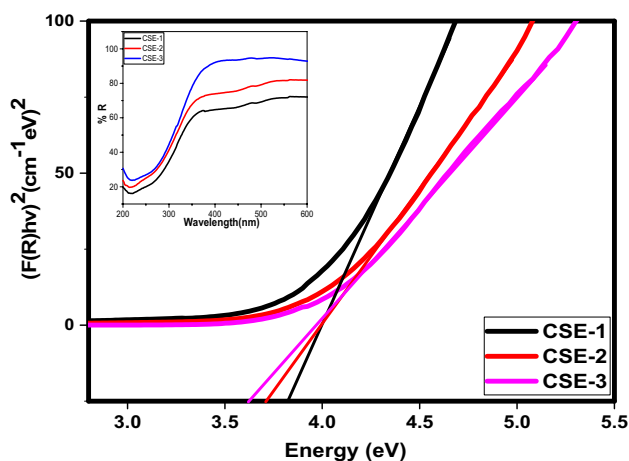


Fig. 5 Optical band gap for all glasses

Table 6 Optical band gap, Urbach energies and refractive indices for all glasses

Glass samples	CSE-1	CSE-2	CSE-3
Band gap (Eg) (eV)	3.84	3.72	3.63
Urbach energy (Eu) (eV)	0.30	0.31	0.34
Refractive index	2.20	2.22	2.24

Eg also depends on the nature and relative concentration of BOs and NBOs. With the increase of ESP, Si–O–Si and P–O–P bonds depolymerize the glass network and produce non-bridging oxygen (NBO). This causes energy gap shifts to lower energies can be due to the formation of NBOs in CSE-1, CSE-2 and CSE-3 glasses. Moreover, the negative charge on NBOs has higher magnitude than BO. When the bridging oxygen is converted into non bridging oxygen then the ionicity of oxygen atoms is increased. Due to this the top of valence band moves up leading to decrease in the band gap with an increase in NBOs [36]. Moreover, the presence of heavy modifiers in glass composition decreases the optical band gap [19].

Reflectance coefficient (F(R) (E)) of the material is related to the Urbach energy as follows [37]:

$$F(R)(E) = A \exp (E/E_u) \tag{5}$$

where, A is a constant called tailing parameter. Urbach energy (E<sub>u</sub>) was determined by taking the reciprocal of the slope of the linear portion of the ln (F(R) (E)) versus energy. The change in Urbach tails can be dependent on many factors like thermal vibrations, dislocations and electric field of defects etc. The higher value of Urbach energy is observed for glass sample CSE-3 and lower energy for glass sample CSE-1 as shown in Table 6. This is also confirmed that CSE-3 glass exhibit more disordering (NBOs etc.) than other

two glasses. This showed again an increase in disorderness as well as an open structure of the glasses due to the formation of non-bridging oxygen. FTIR results also support the above observations.

### 3.6.2 Refractive index

According to Dimitrov and Sumio [38], the refractive index ( $n$ ) of a solid is related to the optical band gap of the material as:

$$\frac{n^2 - 1}{n^2 + 1} = 1 - \sqrt{\frac{E_g}{20}} \quad (6)$$

The density, coordination number, field strength and NBOs of the material are the factors that affect the refractive index of the glass samples [39, 40]. The refractive index is also a structure dependent property. With the increase of ESP, the glass networks of Si–O–Si and P–O–P bonds are depolymerized that produced more NBOs. Baki et al. [41] reported that bridging oxygen's are converted into non-bridging oxygen when more alkaline earth metal ions added. These provide more oxygen to the network. The increase of more NBOs produces more polarizability of oxygen ions which causes increase in the refractive index values. The refractive index is also directly proportional to density. Refractive index of glasses is changed when the structure is changed as it depends on the density. The result of (Table 2) density of present glasses also supports the refractive index. The refractive index increases with  $\text{Fe}_2\text{O}_3$  contents in  $45\text{SiO}_2\text{-}25\text{CaO}\text{-}5\text{P}_2\text{O}_5\text{-}10\text{Na}_2\text{O}\text{-}(15\text{-}x)\text{-MnO}_2\text{-}x\text{Fe}_2\text{O}_3$  glass composition synthesized by minerals [42]. The variation in the refractive index is in good accordance with the changes in the ionic character of the bonds. Increase of more non bridging oxygen's leads to formation of more ionic bond character in spite of covalent character. However, the density, ionic character and polarizability have been the dominating factors for refractive index of the present samples.

### 3.7 Photoluminescence spectroscopic analysis

PL emission bands can be observed at 348, 362, 409, 460, 484, 510, 528 and 542 nm as shown in Fig. 6. The bands 348 nm and 362 nm ascribed from an intrinsic defect in amorphous  $\text{SiO}_2$ . The luminescence from the 348 nm and 362 nm is attributed to silicon dangling bonds developed from E defects centers ( $\text{O}\equiv\text{Si}$ ) being an oxygen vacancy that has trapped hole. This is due to the increase of the ESP contents ( $\text{Ca}^{2+}$ ), some  $\text{Si-O}^-$  bonds disrupts during the process of silica networks associated with non bridging oxygen. Siu et al. [43] observed a UV emission bands at 350 nm and 368 nm corresponds to the defect related luminescence

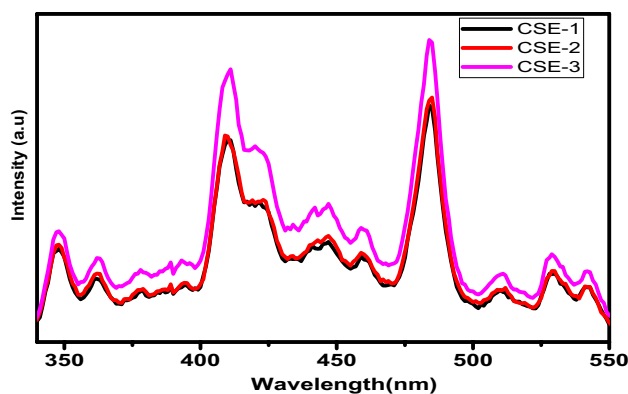


Fig. 6 Photoluminescence spectra for all glasses

centers in  $\text{SiO}_2$ . PL band corresponds to 409 nm for all glasses shows broaden peaks. It is observed from the Fig. 6 that the PL intensities show a similar tendency for 409 nm band. When ESP contents increase the intensity of PL also increases. It may be associated with difference in ionic radii of  $\text{Si}^{4+}$  ( $0.41\text{\AA}$ ) and  $\text{Ca}^{2+}$  ( $0.100\text{\AA}$ ). This could affect the defect centers and structural changes. It also increases the concentration of silicon dangling bonds and oxygen vacancies in the glass networks. These changes are related to the inhomogeneous broadness of PL peaks. The role of CaO in  $\text{SiO}_2\text{-GeO}_2\text{-P}_2\text{O}_5\text{-Er}_2\text{O}_3$  composition has been reported by Acapito et al. [44]. The presence of CaO increases the spectral bandwidth with inhomogeneous broadening of PL spectra.

Fitting PL spectra show four peaks at 410 nm, 422 nm, 445 nm and 460 nm (Fig. 8). The bands lie in range 410–422 nm indicates an extensive distribution of the energy levels that are corresponding to appropriate emission centers. The disturbances in the silica network by trace elements are responsible for this peak [16]. The 410 nm band generally attributed to the characteristic emission of  $\text{Ti}^{4+}$  that is activated through charge-transfer transitions. The transition is taken place from the 2p orbits of the surroundings oxygen ion to empty outer 3d orbit of  $\text{Ti}^{4+}$  in the titanium-oxygen units, i.e.  $\text{O}^{2-}\text{-Ti}^{4+} \rightarrow \text{O}^{2-}\text{-Ti}^{3+}$ . The transition from emitting level  ${}^3\text{T}_2$  or  ${}^3\text{T}_1$  to  ${}^1\text{A}_1$  is responsible for blue PL emission shown in Fig. 7. This band was also reported for conventional glasses,  $\text{TiO}_2$  doped in  $\text{Al}_2\text{O}_3$  [45]. This process of transition from excited  $\text{Ti}^{4+}$  ion to  $\text{O}^{2-}$  ligands exhibit the fluorescent behaviour of  $\text{Ti}^{4+}$  ion in glasses which might be corresponding to the energy transfer by ion-phonon coupling. The band 445 nm in silica glasses corresponds to defects of ODC (Oxygen deficient centre) represented as  $\equiv\text{Si}-\text{Si}\equiv$ . This is also due to the presence of trace element oxide  $\text{TiO}_2$  in the glass samples. The reason is ionic radii of  $\text{Ti}^{4+}$  ( $0.68\text{\AA}$ ) is greater than ionic radii of  $\text{Si}^{4+}$  ( $0.41\text{\AA}$ ) which disrupts the silica



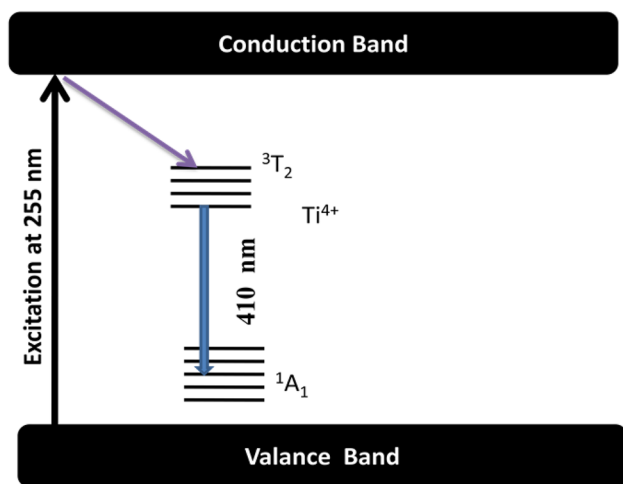


Fig. 7 Band model show Ti<sup>4+</sup> emission mechanism

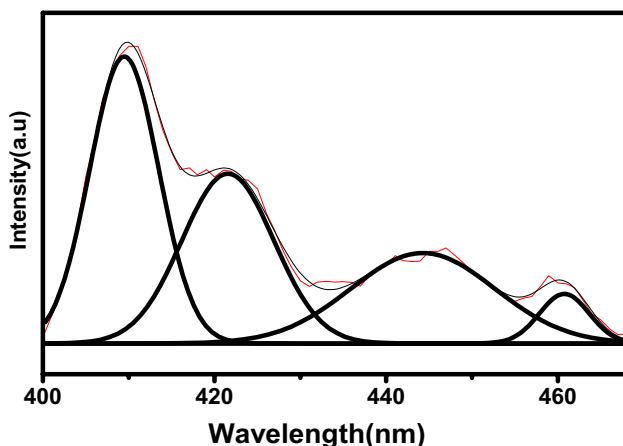


Fig. 8 Deconvolution spectra by peak fitting method using Gaussian curves of glass CSE-1 in the wavelength region from 400 to 470 nm

network that affects the defect concentration and produced radiative transitions [46]. The energy transfer from the defect centers to Ti<sup>4+</sup> that also produced blue emission. TiO<sub>4</sub> is a “self activating” anion which helps to improve the luminescent quality of SiO<sub>2</sub> glasses. A low intensity of the PL band at 460 nm is originated due to diamagnetic radiative recombination of self-trapped excitons (STE) and neutral oxygen vacancies (V<sub>o</sub>). A sharp band at 484 nm is ascribed to the presence of Al<sub>2</sub>O<sub>3</sub> in the glasses. The low intensity of PL bands 510 nm, 528 nm and 542 nm show green emission of light due to the presence of some trace element oxides. This also depends on the excitation power and characteristics of radiative recombination of STE. Two photoluminescence bands at 420–430 nm and 510 nm are observed in when ZnS doped with TiO<sub>2</sub> due to Ti<sup>3+</sup> and Ti<sup>4+</sup> precipitation, which leads to excitonic emissions and trapped luminescence [47].

### 3.7.1 CIE coordinates and color purity

The Commission International de l’Eclairage (CIE) 1931 XY chromaticity co-ordinate diagram was plotted using emission spectra to determine the color purity of CSE-3 glass (Fig. 9). The CIE co-ordinates for CSE 3 glass was observed (x = 0.17, y = 0.23) respectively, which lies in the greenish-blue region. Finally, the color purity of CSE-3 glass was determined using Eq. (7). The color purity of a light source is the distance in the chromaticity diagram between the (x, y) color coordinate point of the test source and the coordinate of the equal energy point divided by the distance between the equal energy point and the dominant wavelength point.

The color purity is thus given by following equation:

$$\text{Color purity (\%)} = \frac{\sqrt{(x - x_i)^2 + (y - y_i)^2}}{\sqrt{(x_d - x_i)^2 + (y_d - y_i)^2}} \times 100 \quad (7)$$

where, (x, y), (x<sub>i</sub>, y<sub>i</sub>) and (x<sub>d</sub>, y<sub>d</sub>) represent the chromaticity coordinates of the light source under test, equal-energy reference illuminant with a value of (x<sub>i</sub> = 0.3333, y<sub>i</sub> = 0.3333) and dominant-wavelength coordinates (x<sub>d</sub>, y<sub>d</sub>) respectively [48]. The color purity was determined by putting the coordinates of (x, y), (x<sub>d</sub>, y<sub>d</sub>) and (x<sub>i</sub>, y<sub>i</sub>) to Eq. (7). The color purity of the sample CSE-3 was 66%. In case of agro-food waste derived glasses, particularly at room temperature showed the optimal intensity of photoluminescence and 66% of color purity due to the charge transfer by coupling between ions and phonons. In case of mineral glasses same may not take place probably at room temperature. Agro-food wastes derived glasses exhibit some advantages over conventional

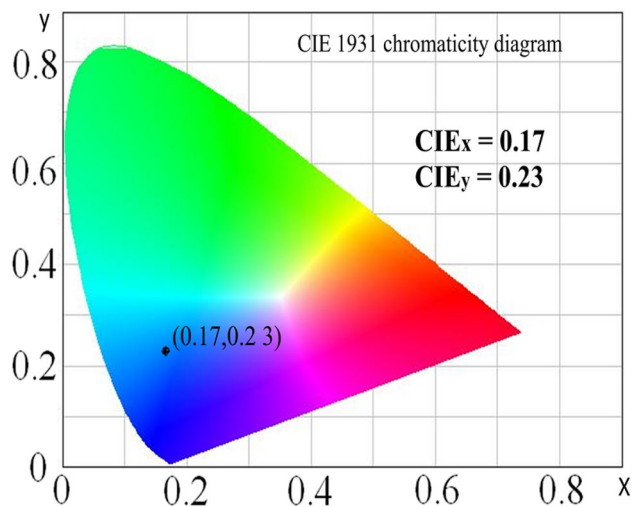


Fig. 9 Colour coordinates calculated from emission spectra

glasses. The presence of an inherent trace element oxides acts as PL activator in host glass matrix. However, in case of mineral based glasses some rare-earth PL activator must be added for deriving PL. It will be very interesting to study the effect of rare-earth elements in agro-food waste derived glasses and glass–ceramics for further modify and enhance the PL luminescence of agro-food waste derived glasses.

## 4 Conclusion

Agro-food wastes are used to synthesize glasses. XRD confirmed the amorphous nature of agro-food waste derived samples. The density of the glasses increased with increase of ESP (CaO) contents. The density of these glasses is lower to the similar glasses formed from minerals. The addition of ESP (CaO) increases the hydrophilic nature of the glasses. All the glass exhibit all four structural units of  $\text{SiO}_2$  i.e.  $Q^0$ ,  $Q^1$ ,  $Q^2$ ,  $Q^3$  and  $Q^4$ . However, the addition of ESP increases  $Q^0$ ,  $Q^1$  and  $Q^2$  structural unit. The optical band gap lay in wide semiconductor range and decreases with the increase of the ESP contents due to more NBO's in the glasses. Vickers micro hardness is higher than the earlier reported hardness of the mineral based glasses. The high refractive index and Urbach energy observed for CSE-3 glass as compared to other two glasses. PL spectra showed greenish-blue emission peaks with 66% of color purity. The peak intensity increases with CaO contents. The trace elements act as 'self activator' center to generate PL. These synthesized samples can be used in the lamp industry, especially for solid state lighting (mercury free lamps) and LEDs.

**Acknowledgements** This research did not receive any specific grant from funding agencies in the public, commercial, or not-for-profit sectors. Authors are very thankful to SAI labs for carrying out the EDS of the samples. The author is also thankful to Dr. Devinder Kumar for Vickers hardness measurement and Gaurav Sharma for their consistent guidance and support to carry out this work.

## References

1. R.A. Patil, U.B. Deshannavar, Dry sugarcane leaves: renewable biomass resources for making briquettes. *Int. J. Eng. Res. Technol.* **10**, 232–235 (2017)
2. S. Chandershekhar, K.G. Satyanarayana, P.N. Pramada, P. Raghavan, T.N. Gupta, Properties and applications of reactive silica from rice husk-an overview. *J. Mater. Sci.* **8**, 3159–3168 (2003)
3. S. Kumar, P. Sangwan, R.M.V. Dhankhar, S. Bidra, A review: utilization of rice husk and their ash. *Res. J. Chem. Environ. Sci.* **1**, 126–129 (2013)
4. K. Mohanta, D. Kumar, O. Parkash, Properties and industrial applications of rice husk: a review. *Int. J. Emerg. Technol. Adv. Eng.* **2**, 86–90 (2012)
5. M.Z. Norashikin, M.Z. Ibrahim, The potential of natural waste (corn husk) for production of environmental friendly biodegradable film for seedling world. *Acad. Sci. Eng. Technol.* **3**, 1802–1806 (2009)
6. I.A. Cornejo, S. Ramalingam, J.S. Fish, I.E. Reimanis, Hidden treasures: turning food waste into glass. *Am. Ceram. Soc. Bull.* **93**, 24–27 (2014)
7. R. Embong, N. Shafiq, A. Kusbiantor, Silica extraction and incineration process of sugarcane bagasse ash as poolanis materials: a review. *J. Eng. Appl. Sci.* **11**, 7304–7308 (2016)
8. K.G. Patel, R.R. Shettigar, N.M. Misra, Recent advance in silica production technologies from agricultural waste stream:Review. *J. Adv. Agri. Technol.* **4**, 274–279 (2017)
9. R.K. Brow, Review: the structure of simple phosphate glasses. *J. Non-Cryst. Solids* **1**, 1–28 (2000)
10. N.G. Boetti, D. Pugliese, E. Ceci-Ginistrelli, J. Lousteau, D. Janner, D. Milanese, Highly doped phosphate glass fibers for compact lasers and amplifiers. *Appl. Sci.* (2017). <https://doi.org/10.3390/app7121295>
11. T.L. Arinze, T. Tran, J. McAlary, G. Daculsi, A comparative study of biphasic calcium phosphate ceramics for human mesenchymal stem-cell-induced bone formation. *Biomaterials* **26**, 3631–3638 (2005)
12. W. Ahmina, M. El. Moudane, M. Zriouil, M. Taibi, Role of manganese in  $20\text{K}_2\text{O-xMnO-(80-x)P}_2\text{O}_5$  phosphate glasses and model of structural units. *J. Mater. Environ. Sci.* **7**, 694–699 (2016)
13. Z. Teixeira, O.L. Alves, I.O. Mazali, Structure, thermal behavior, chemical durability, and optical properties of the  $\text{Na}_2\text{O-Al}_2\text{O}_3\text{-TiO}_2\text{-Nb}_2\text{O}_5\text{-P}_2\text{O}_5$  glass system. *J. Am. Ceram. Soc.* **90**, 256–263 (2007)
14. I. Audulrahman, H.I. Tijani, B.A. Mohammed, H. Saidu, H. Yusuf, M.N. Jibrin, S. Mohammed, From garbage to biomaterials: an overview on egg shell based hydroxyapatite. *J. Mater.* (2014). <https://doi.org/10.1155/2014/802467>
15. S.S. Danewalia, G. Sharma, S. Thakur, K. Singh, Agricultural wastes as a resource of raw materials for developing low-dielectric glass-ceramics. *Sci. Rep.* **6**, 1–12 (2016)
16. G. Sharma, S.K. Arya, K. Singh, Optical and thermal properties of glasses and glass-ceramics derived from agricultural wastes. *Ceram. Int.* **44**, 947–952 (2018)
17. L.L. Devi, C. Basavapoornima, V. Venkatramu, P. Babu, C.K. Jayasankar, Synthesis of  $\text{Ca}_2\text{SiO}_4\text{:Dy}^{3+}$  phosphors from agricultural waste for solid state lighting applications. *J. Ceram. Int.* **43**, 16622–16627 (2017)
18. L.L. Devi, C.K. Jayasankar, Spectroscopic investigations on high efficiency deep red-emitting of  $\text{Ca}_2\text{SiO}_4\text{:Eu}^{3+}$  phosphors synthesized from agricultural waste. *J. Ceram. Int.* (2018). <https://doi.org/10.1016/j.ceramint.2018.05.003>
19. B. Aktas, M. Albaskrara, S. Yalcin, K. Dogru, Optical properties of soda-lime-silica glasses doped with peanut shell powder. *Acta Phys. Pol. A* **131**, 57–61 (2016)
20. B. Aktas, M. Albaskrara, K. Dogru, S. Yalcin, Optical Properties of Soda-lime-silica glasses doped with eggshell powder. *Acta Phys. Pol. A* **132**, 442–444 (2017)
21. S.R. Teixeira, A.E. Souza, C.L. Carvialho, V.C.S. Reynoso, M. Romero, J.M. Rincon, Characterization of a wollastonite glass-ceramic material prepared using sugar cane bagasse ash (SCBA) as one of the raw materials. *Mater. Charact.* **98**, 209–214 (2014)
22. S. Singh, K. Singh, Nanocrystalline glass ceramics: structural, physical and optical properties. *J. Mol. Struct.* **1081**, 211–216 (2015)
23. A. Balamurugan, G. Balossier, J. Michel, S. Kannan, H. Benhayoune, A.H.S. Rebelo, J.M.F. Ferreira, Sol gel derived  $\text{SiO}_2\text{-CaO-MgO-P}_2\text{O}_5$  bioglass system—Preparation and in vitro characterization. *J. Biomed. Mater. Res. B* (2007) 546–553
24. A.M. Efimov, V.G. Pogareva, IR absorption spectra of vitreous silica and silicate glasses: The nature of bands in the 1300 to 5000  $\text{cm}^{-1}$ . *Region. Chem. Geol.* **229**, 198–217 (2006)

25. K. Singh, I. Bala, V. Kumar, Structural, optical and bioactive properties of calcium borosilicate glasses. *Ceram. Int.* **35**, 3401–3406 (2009)
26. H.R.A. Mooghari, A. Nemati, B.E. Yekta, Z. Hamnabar, The effects of SiO<sub>2</sub> and K<sub>2</sub>O on glass forming ability and structure of CaO-TiO<sub>2</sub>-P<sub>2</sub>O<sub>5</sub> glass system. *Ceram. Int.* **38**, 3281–3290 (2012)
27. G. Melinte, L. Baia, V. Simon, Hydrogen peroxide versus water synthesis of bioglass-nanocrystalline hydroxyapatite composites. *J. Mater. Sci.* **46**, 7393–7400 (2011)
28. R. Hussin, M.A. Salim, N.S. Alias, M.S. Abdullah, S. Abdullah, S.A.A. Fuzi, S. Hamdan, M.N.M. Yusuf, Vibrational studies of calcium magnesium ultra phosphate glasses. *J. Fund. Sci.* **5**, 41–53 (2009)
29. A.M. Handke, W. Mozgawa, M. Nocun, Specific features of the IR spectra of silicate glasses. *J. Mol. Struct.* **325**, 129–136 (1994)
30. R.P. Smith, The relationship of force constant and bond length. *J. Phys. Chem.* **60**(9), 1293–1296 (1956)
31. M.M. Smedskjaer, M. Jensen, Y. Yue, Effect of thermal history and chemical composition on hardness of silicate glasses. *J. Non-cryst. Solids.* **356**, 893–897 (2010)
32. J.E. Shelby, *Introduction to Glass Science and Technology*, 2nd edn. (The Royal Society of Chemistry, UK, 2005)
33. G.V. Rao, H.D. Shashikala, Optical and mechanical properties of calcium phosphate glasses. *Glass Phys. Chem.* **40**, 303–309 (2014)
34. P. Jha, K. Singh, Effect of MgO on bioactivity, hardness, structural and optical properties of SiO<sub>2</sub>-K<sub>2</sub>O-CaO-MgO glasses. *Ceram. Int.* **42**, 436–444 (2016)
35. P. Kubelka, F. Munk, Ein Beitrag zur Optik der Farbanstriche. *Zeits. f. techn. Physik* **12**, 593–601 (1931)
36. J.A. Duffy, The glass is doped with ZnO to tune the glass absorption glasses. *Phys. Chem.* **42**, 151 (2001)
37. F. Urbach, The long-wavelength edge of photographic sensitivity and of the electronic absorption of solids. *Phys. Rev.* **92**, 1324 (1953)
38. V. Dimitrov, S. Sumio, Electronic oxide polarizability and optical basicity of simple oxides. *J. Appl. Phys.* **79**, 1736 (1996)
39. A.S. Hassanien, A.A. Akl, Optical characteristics of iron oxide thin films prepared by spray pyrolysis technique at different substrate temperatures. *Appl. Phys. A* **124**, 752 (2018)
40. A. S. Hassanien, Studies on dielectric properties, Opto-electrical parameters and electronic polarizability of thermally evaporated amorphous Cd50 S50-xSe x thin films, *J. Alloys Compd.* **671** (2016) 566–578
41. M.A. Baki, F.A. Wahab, A.A. Radi, F. El-Diasty, Factors affecting optical dispersion in borate glass systems. *J. Phys. Chem. Solids* **68**, 1457–1470 (2007)
42. S. Singh, K. Singh, Effect of in-situ reduction of Fe<sup>3+</sup> on physical, structural and optical properties of calcium sodium silicate glasses and glass ceramics. *J. Non-Cryst. Solids* **386**, 100–104 (2014)
43. G.G. Siu, X.L. Wu, Y. Gu, X.M. Bao, Ultraviolet and blue emission from crystalline SiO<sub>2</sub> coated with LiNbO<sub>3</sub> and LiTaO<sub>3</sub>. *Appl. Phys. Lett.* **74**, 1812–1814 (1999)
44. F.D. Acapito, C. Maurizio, M.C. Paul, T. Lee, W. Blanc, Role of CaO addition in the local order around Erbium in SiO<sub>2</sub>-GeO<sub>2</sub>-P<sub>2</sub>O<sub>5</sub> fiber performs. *Mater. Sci. Eng. B.* **146**, 167–174 (2008)
45. H.H. Kusuma, Z. Ibrahim, UV-spectroscopy and band structure of Ti: Al<sub>2</sub>O<sub>3</sub>. *J. Solid State Sci. Technol.* **20**, 41–47 (2012)
46. C.F. Song, M.K. Lu, S.F. Wang, D. Xu, D.R. Yuan, G.J. Zhou, Blue photoluminescence of sol-gel TiO<sub>2</sub>-SiO<sub>2</sub> glass. *J. Inorg. Mater.* **39**, 1529–1531 (2003)
47. P. Yang, C.F. Song, M.K. Lu, D. Xu, D.R. Yuan, G.J. Zhou, The effect of alkaline earth metallic ions on the photoluminescence properties of sol-gel silica glasses. *Appl. Phys. A.* **74**, 689–692 (2002)
48. T. Smith, J. Guild, The C.I.E colorimetric standards and their use. *Trans. opt. Soc.* **33**, 73 (1931)